Modelling and Simulation in Materials Science and Engineering 2013, 21(085012)

A modified level set approach to 2D modeling of dynamic recrystallization

Håkan Hallberg
Division of Solid Mechanics
Lund University, Box 118, S-221 00 Lund, Sweden
hakan.hallberg@solid.lth.se

Abstract

The macroscopic properties of metallic materials depend on the state of the grain microstructure. Recrystallization acts as one of the most important mechanisms in the evolution of the microstructure and hence also of the macroscopic properties. The present paper presents a mesoscale model of microstructure evolution due to recrystallization, based on a level set formulation employed in a finite element setting. The use of level sets to represent grains and grain boundaries in polycrystal microstructures is a relatively recent development in computational materials science and the present contribution suggests new methodologies such as interface reconstruction, allowing for example boundary conditions to be prescribed along grain boundary interfaces and distinct localization and representation of grain boundary junctions. Polycrystal plasticity is modeled by considering the evolution of dislocation density in the individual crystals. The influence of grain boundaries on dislocation accumulation is captured in the model, causing the formation of dislocation density gradients within the grains. The model is used in simulations of dynamic recrystallization, taking pure copper as example material. It is shown that the proposed model captures the salient features of dynamic recrystallization during thermomechanical materials processing.

Keywords: Level set, Recrystallization, Dislocation density, Grain size, Gradients

1 Introduction

The macroscopic behavior of metallic materials is to a large extent controlled by the state of the grain microstructure. The microlevel grain structure will influence macroscopic

DOI: 10.1088/0965-0393/21/8/085012

material properties such as strength, hardness, ductility and resistance against fatigue and corrosion. Being able to predict and control the evolution of this microstructure, for example in terms of grain size, during thermomechanical processing of the material allows the development of tailored material properties, optimized products and more efficient production processes. Understanding and manipulating the material microstructure are key components in the production of functionally graded materials, having engineered properties in different regions and in the production of modern high-strength steels.

Recrystallization is the main mechanism to control the evolution of grain microstructures and is generally accepted to be defined as the formation of a new grain structure in a cold-worked material, occurring through the formation and migration of high-angle boundaries. The grain boundary migrations are mainly driven by stored energy reduction and minimization of grain boundary surface energy.

During thermomechanical processing of metallic materials, i.e., when the material is exposed to plastic deformation at elevated temperatures, stored energy increase through dislocation accumulation and stored energy reduction through nucleation of new grains work in parallel. This process is commonly labelled *dynamic recrystallization* (DRX) [1, 2]. The process of DRX is sometimes further subdivided into a relatively slow *continuous dynamic recrystallization* (CDRX) or a more rapidly progressing *discontinuous dynamic recrystallization* (DDRX) [3, 4, 5]. In materials of low stacking-fault energy, such as copper, dynamic recovery processes such as cross slip and climb are less influential and the recrystallization is dominated by DDRX during which new grains are nucleated as regions of low dislocation density that may grow to consume the more dislocation-dense surrounding matrix material. DDRX will be most significant in the microstructure regions having the highest dislocation density, primarily at grain boundary triple junctions and along grain boundaries but also at inclusions and along slip bands in the grain interiors.

An array of numerical algorithms have been used in modeling of microstructure evolution during recrystallization. A review of some of the most significant methods is given in [6]. Historically, *Monte Carlo Potts* (MCP) algorithms have been used to simulate recrystallization – mainly static recrystallization – in both 2D and 3D on fixed computational grids. The system energy is minimized through probabilistic changes to the state variables, defined at the grid points [7, 8].

An alternative method is given by *cellular automata* (CA) which have been employed frequently in studies on both static and dynamic recrystallization [9, 10, 11, 12]. As with MCP models, CA models are also usually defined on fixed grids, but use physical cell state switching conditions, based on recrystallization kinetics. The cell state switching can, however, be performed as either deterministic or probabilistic. While CA algorithms perform time integration using physical time, this is not possible in MCP models where "Monte Carlo steps" are used as a measure of time. This makes comparison between MCP results and experimental results cumbersome.

The curvature of interfaces is an important aspect of grain boundary migration kinetics but being based on discrete grids with no direct representation of interface curvature, both MCP and CA algorithms have shortcomings in this respect. The choice of grid type (square, hexagonal etc.) also influence the grain growth kinetics and may be detrimental to the simulation results. A remedy for such grid dependence is to use random grids, as discussed in [11]. In addition, both MCP and CA are computationally efficient and 3D implementations are straight-forward. Both methods also scale well when subject to computer parallelization.

Interface migration can also be described by *front tracking* or *vertex models* where the migration kinetics of grain boundary triple junctions are considered [13, 14, 15, 16, 17]. Grain topology is represented by nodes placed at the triple junctions. The representation of curvature, however, comes with additional computational cost as intermediate nodes have to be introduced between the triple junctions. In addition, the extension of the method to 3D is not easily realized, requiring surface tesselations. Also, topological changes to the grain structure requires dealing with different transformation conditions.

Phase-field methods (PF) have received significant interest in recent years in simulations of a broad spectrum of physical processes, including recrystallization [18, 19, 8, 20, 21]. In PF models of recrystallization, the grain microstructure is described by phase field variables. These are functions that are continuous in space and a distinction is made between conserved and non-conserved variables. A conserved variable is typically a measure of the local composition whereas a non-conserved variable contains information on the local structure and could represent for example the crystallographic orientation. Within a single grain, a phase field variable maintains a nearly constant value that correspond to the properties of that grain. Grain boundaries are represented as interfaces where the value of the phase field variable gradually varies between the values in the neighboring grains on opposing sides of the grain boundary. Grain boundaries are hence described as diffuse transition regions of the phase field variables. The computational effort in treating the rapidly changing fields across diffuse interfaces can be considerable and the formulation of the energy densities to capture physical microstructure features is not trivial. In addition, topological changes such as nucleation of new grains are not easily handled.

The *level set* formulation was introduced in [22] as a numerical tool to trace the spatial and temporal evolution of interfaces. The method was later extended to consider interfaces with multiple junctions in [23, 24]. The advantages of the level set methodology in representation of grain microstructures, with application to recrystallization simulation, are discussed in [25, 26, 27]. Coupling of a crystal plasticity finite element model with a level set formulation of recrystallization is presented in [28]. A level set approach to microstructure evolution is also taken in [29, 30] where finite difference schemes are used on fixed grids, in both two and three dimensions. In these publications, some simplifications are made, for example in terms of the treatment of plasticity. Some of the models consider grain

boundary migration as only curvature-driven or, alternatively, as driven solely by stored energy differences. As noted in [24, 31], standard level set formulations do not correctly capture the interaction between multiple grains, occurring for example at grain boundary triple junctions, and corrections have to be implemented to remedy this shortcoming.

The present model is set within a level set framework where modifications are introduced in the discretization of the grain boundaries. The employed interface reconstruction allows boundary conditions to be applied along grain boundaries and also permits distinct localization of grain boundary triple junctions using isogonic points. This methodology enforces local equilibrium configurations of the boundaries that meet at the junctions. Considering the evolution of polycrystal plasticity, the dislocation density is introduced as a parameter, defining the dislocation density within each individual grain. A simple method is devised in the present model to make the evolution of the dislocation density within a grain sensitive to the presence of – and distance to – the grain boundary. This allows dislocation accumulation at grain boundaries to be captured, resulting in stored energy gradients within the grains. Since the dislocation density will be concentrated primarily along grain boundaries, appropriate nucleation sites for dynamic recrystallization emerge naturally from the model.

Taking pure copper as example material, a 2D model is formulated as a representative area element. This model is used to perform simulations of thermomechanical materials processing, showing the capabilities of the proposed formulation. It is shown that both the simulated microstructure and the resulting macroscopic, homogenized, material response correspond well to experimental data on pure copper, taken from the literature.

This paper is divided into sections with Section 2 establishing the level set framework and Section 3 describing the necessary aspects of recrystallization kinetics. In Section 4, details of level set modeling of recrystallization are given and in Section 5 the methodology for interface reconstruction is detailed. The description of polycrystal plasticity and modeling of dislocation density gradients is discussed in Section 6. Using the proposed interface reconstruction, the refinement of the finite element mesh along grain boundaries can be controlled. This is employed in Section 7 where the mesh refinement required to capture interface kinetics is determined. In Section 8, the proposed model is applied to simulations of thermomechanical processing of copper to describe the microstructure evolution and the macroscopic material response. Some concluding remarks closes the paper in Section 9.

2 Level set framework

Since the level set method was introduced by Osher and Sethian in [22], it has been employed in numerical simulations of a vast number of physical and chemical processes where there is a need for tracing the evolution of interfaces.

The starting point is the definition of a level set function $\phi(\boldsymbol{x}, t)$ on a domain Ω, where

$\boldsymbol{x}$ are the spatial coordinates and t the time. The spatial discontinuity Γ, i.e., the interface, is identified as the zero-level contour where $\phi = 0$. In addition, the level set is taken as a distance function, for any point $\boldsymbol{x}$ representing the distance $d(\boldsymbol{x}, t, \Gamma)$ to the interface Γ at a certain time. A sign convention is adopted, defining $\phi > 0$ inside Γ, $\phi < 0$ outside of the interface and $\phi = 0$ at the interface. We thus have

$$\begin{cases} \phi(\boldsymbol{x}, t) = d\left(\boldsymbol{x}, t, \Gamma\right), \ \boldsymbol{x} \in \Omega \\ \Gamma = \{\boldsymbol{x} \in \Omega, \ \phi(\boldsymbol{x}) = 0\} \end{cases} \tag{1}$$

Since $\phi(\boldsymbol{x}, t)$ is taken as a signed distance function, it holds that

$$\|\boldsymbol{\nabla}\phi(\boldsymbol{x}, t)\| = 1, \quad \boldsymbol{x} \in \Omega \tag{2}$$

It is also noted that the local interface normal $\boldsymbol{n}$ and the interface curvature κ are conveniently obtained from the level set function by evaluating

$$\begin{cases} \boldsymbol{n} = \dfrac{\boldsymbol{\nabla}\phi}{\|\boldsymbol{\nabla}\phi\|} \equiv \boldsymbol{\nabla}\phi, \\ \kappa = \boldsymbol{\nabla}^{\mathrm{T}}\boldsymbol{n} \equiv \boldsymbol{\nabla}^{\mathrm{T}}\left(\dfrac{\boldsymbol{\nabla}\phi}{\|\boldsymbol{\nabla}\phi\|}\right) \equiv \boldsymbol{\nabla}^2\phi \equiv \Delta\phi, \end{cases} \quad \text{if} \quad \|\boldsymbol{\nabla}\phi\| = 1 \tag{3}$$

Stationarity of the level set field requires that

$$\frac{D\phi}{Dt} = 0 \quad \Rightarrow \quad \frac{\partial\phi}{\partial t} + \left(\boldsymbol{\nabla}^{\mathrm{T}}\phi\right)\frac{\partial \boldsymbol{x}}{\partial t} = 0 \tag{4}$$

Taking advantage of the interface normal in eq. (3a), the interface velocity v_n, normal to the interface, can be expressed as

$$\boldsymbol{v} = v_n\boldsymbol{n} \tag{5}$$

So far a single interface was considered. To handle situations with multiple interfaces, a generalization of the level set formulation was presented in [23]. By this approach, and considering a total of N_ϕ individual level sets, the evolution of the level set functions can be stated as a Hamilton-Jacobi formulation according to

$$\begin{cases} \dfrac{\partial\phi_i}{\partial t} + \boldsymbol{v}^{\mathrm{T}}\boldsymbol{\nabla}\phi_i = 0, \\ \phi_i(t = 0, \boldsymbol{x}) = \phi_i^0(\boldsymbol{x}), \end{cases} \quad \forall \ i \in \{1...N_\phi\} \tag{6}$$

where $\phi_i^0(\boldsymbol{x})$ are the initial positions of the interfaces at time $t = 0$.

Further considering a total of N_ϕ level sets, a global unsigned level set $\phi_{\mathrm{glob}}(\boldsymbol{x})$ can be constructed from

$$\phi_{\mathrm{glob}}(\boldsymbol{x}) = \max\left\{\phi_i(\boldsymbol{x}), \ 1 \leq i \leq N_\phi\right\} \tag{7}$$

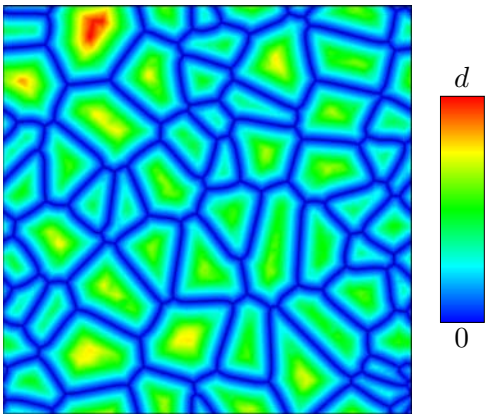

Figure 1: Illustration of the global level set ϕ_{glob} in eq. (7), representing the distance d from the grain boundary in each grain.

The global level set in eq. (7) is illustrated in Fig. 1 for a domain representing a polycrystal with the individual grains being defined by level sets. Fig. 1 shows how the level sets represent the distance d from the grain boundary to any point within the individual grains.

2.1 Level set interaction correction

To avoid kinematic incompatibilities when multiple level sets are considered – i.e., the development of voids and overlaps between adjacent level sets – an interaction correction step is usually repeatedly performed at some interval during the solution of eq. (6). Following [23], this correction can be achieved by, at all points $\boldsymbol{x}$, modifying all level sets according to

$$\phi_i = \frac{1}{2}\left(\phi_i - \max_{j \neq i}\left(\phi_j\right)\right), \quad \forall\, i, j \in \{1...N_\phi\} \tag{8}$$

It is noted that vacuum regions, that is regions where all $\phi_j < 0$, tend to still be present at junctions where multiple interfaces meet, even after interaction correction according to eq. (8), cf. [24, 31]. The size of these vacuum regions depends on the resolution of the underlying grid or mesh. This is a shortcoming of standard level set formulations which is addressed in the present work as part of the interface reconstruction technique, discussed in Section 5.

2.2 Level set reinitialization

In solving eq. (6), there is a tendency for the level sets to drift from keeping the property of a signed distance function. This is especially the case for irregular interfaces and hetero-

geneous interface velocities. To address this, different remedies have been proposed, often involving solving an Eikonal equation based on eq. (6), cf. [32, 33, 34, 35].

If only the evolution of the interfaces is of interest, the reinitialization need not be performed over the entire domain Ω, only in the vicinity of the interfaces. In the present case, however, the introduction of dislocation density gradients, discussed in Section 6, takes advantage of the level sets keeping the property of a signed distance function throughout the domain. To this end, and for convenient implementation, the level sets are in the present formulation reinitialized, or redistanced, by a direct approach. This is achieved by dividing the zero contour of each level set into segments and then calculating the distance from each nodal point in the finite element mesh to each segment. This choice of reinitialization formulation is further motivated since the division of interfaces into segments is also employed in the interface reconstruction discussed in Section 5.

Considering the situation shown in Fig. 2, the present reinitialization algorithm consists of the following steps:

1. Define an interface segment by its end points A and B, based on the computational discretization of the domain.

2. Calculate the normal direction from any point C, orthogonal to the segment, considering two possible cases:

   - If the normal line intersects within the segment, then the calculated distance between points C and D is taken as the distance from point C to the interface.
   - If the line does not intersect within the segment, the shortest distance between point C and any of the end points A and B is taken as the distance from point C to the interface.

3. Minimize all possible distances from point C to all interface segments to obtain the reinitialized value.

4. Repeat steps (1)-(3) for all segments comprising the interface of a single grain.

By this approach, the geometry of grain boundaries is directly represented by a set of vertices, pair-wise connected by line segments.

3 Recrystallization kinetics

During cold working of metallic materials the stored energy will increase, mainly due to the accumulation of dislocations. The microstructure of the material will be in a state of thermodynamic instability and recrystallization may occur to revert the material to a more stable state. Recrystallization is generally viewed as a process whereby new grains

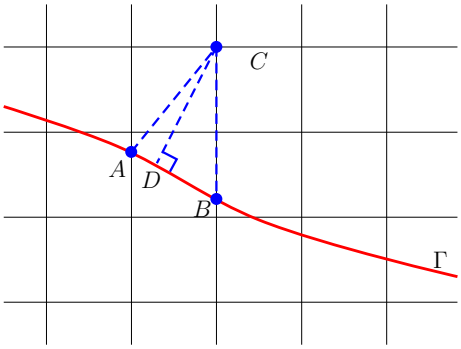

Figure 2: Principle for direct calculation of the distance from a point C to an interface Γ.

nucleate as region in the microstructure that are relatively free of dislocations and hence also of low energy. The nuclei can grow by migration of high-angle boundaries to consume the surrounding cold worked grain structures.

The velocity of migrating boundaries is usually described by the kinetics relation

$$\boldsymbol{v} = mp\boldsymbol{n} \tag{9}$$

where m is the grain boundary mobility, p the driving pressure acting on the boundary and $\boldsymbol{n}$ the local grain boundary normal. Following [2], the driving pressure appears as

$$p = [\![E_\mathrm{s}]\!] - \gamma\kappa \tag{10}$$

where γ is the grain boundary energy and κ the local grain boundary curvature. The jump in stored energy across the interface, $[\![E_\mathrm{s}]\!]$, can be obtained from the corresponding jump in dislocation density across the interface by evaluating

$$[\![E_\mathrm{s}]\!] = \tau[\![\rho]\!] \tag{11}$$

In eq. (11), the dislocation line tension was introduced as $\tau = \mu b^2/2$, b and μ being the magnitude of the Burgers vector and the shear modulus, respectively. From eq. (10) it is evident that grain growth will occur under a competing process of stored energy reduction and grain boundary energy minimization.

The grain boundary mobility m, appearing in eq. (9), can be written as

$$m\left(T\right) = m_0\left(T\right)\exp\left(\frac{-Q_\mathrm{m}}{RT}\right) \tag{12}$$

where Q_m is the activation energy for grain boundary migration, R the gas constant and T the absolute temperature. From the Turnbull estimate [36, 37], the pre-exponential factor appears as

$$m_0\left(T\right) = \beta\frac{\delta D_\mathrm{gb} V_\mathrm{m}}{b^2 RT} \tag{13}$$

where δ, D_{gb} and V_{m} are the mean grain boundary width, grain boundary diffusivity and molar volume, respectively. The Turnbull estimate can be considered as an upper limit to the grain boundary mobility and following [38], the model parameter $0 < \beta \leq 1$ is introduced in eq. (13) to allow scaling of the mobility to comply with the behavior of a particular material. It is noted that different boundaries may have different mobilities due to the local content of solute atoms and due to the misorientation across the interface and the inclination of the boundary plane. For simplicity, such dependencies are not considered in the boundary mobilities in the present model. Hence, all boundaries are considered to possess the same mobility at a given temperature.

The grain boundary energy γ was introduced in eq. (10). This energy varies with the grain boundary configuration in terms of crystallographic misorientation θ across the interface and the orientation of the boundary plane. The grain boundary energy is usually taken to obey the Read-Shockley relation for low-angle boundaries (LAGB) and held at a constant value for high-angle boundaries (HAGB) [39, 2]. By this approach, the grain boundary energy is given by

$$\gamma = \begin{cases} \gamma_{\mathrm{m}} \dfrac{\theta}{\theta_{\mathrm{m}}} \left[1 - \ln \left(\dfrac{\theta}{\theta_{\mathrm{m}}} \right) \right] & \text{for} \quad \theta \leq \theta_{\mathrm{m}} \\ \gamma_{\mathrm{m}} & \text{for} \quad \theta > \theta_{\mathrm{m}} \end{cases} \tag{14}$$

Here, γ_{m} is the grain boundary energy for HAGB and θ_{m} the scalar misorientation differentiating between LAGB and HAGB, often approximated as $\theta_{\mathrm{m}} = 15°$. In the present model all recrystallization nuclei are assumed to emerge with high-angle boundaries, $\theta \geq \theta_{\mathrm{m}}$, with respect to their neighbors and a constant value of the grain boundary energy γ is used.

4 Level set modeling of recrystallization

Considering level sets applied to modeling of recrystallization, the interface velocity $\boldsymbol{v}$ appearing in eq. (6) is with eqs. (9) and (10) given by

$$\boldsymbol{v} = \boldsymbol{v}_\rho + \boldsymbol{v}_\kappa \tag{15}$$

with the following interface velocity quantities being introduced

$$\begin{aligned} \boldsymbol{v}_\rho &= v_\rho \boldsymbol{n}, \quad & v_\rho &= m [\![E_{\mathrm{s}}]\!]_{ij} \\ \boldsymbol{v}_\kappa &= v_\kappa \kappa \boldsymbol{n}, \quad & v_\kappa &= -m\gamma \end{aligned} \tag{16}$$

where $[\![E_{\mathrm{s}}]\!]_{ij}$ is the jump in stored energy across the boundary between grains i and j. Taking advantage of eq. (3), and assuming that $\|\boldsymbol{\nabla}\phi_i\| = 1$ holds due to level set reinitialization, this allows eq. (6) to be reformulated as

$$\begin{cases} \dfrac{\partial \phi_i}{\partial t} + \boldsymbol{v}_\rho^{\mathrm{T}} \boldsymbol{\nabla} \phi_i + v_\kappa \boldsymbol{\nabla}^2 \phi_i = 0, & \forall\ i \in \{1 ... N_\phi\} \\ \phi_i(\boldsymbol{x}, t = 0) = \phi_i^0(\boldsymbol{x}), \end{cases} \tag{17}$$

The resulting formulation in eq. (17) constitutes a transient advection/convection-diffusion equation that in the present implementation is solved in a finite element setting.

4.1 Estimation of the convective velocity field due to stored energy differences

Whereas the diffusion-part of the velocity in eq. (16b) follows from the curvature κ of the level set, the convective velocity $\boldsymbol{v}_\rho$ due to stored energy jumps, cf. eq. (16a), requires some additional attention. This velocity field has to be constructed in such way that discontinuities in the velocity field are avoided at junctions where the boundary normals are not continuously defined.

Due to the interface reconstruction proposed in Section 5, a subset of the nodes in the finite element mesh will coincide with the grain boundaries. At each of these interface nodes, all level sets having a zero value there are considered. This will involve two level sets at nodes along regular boundaries and three level sets at triple junction nodes. These level sets are collected in the set $\widetilde{N}_\phi$. The velocity $\boldsymbol{v}_\rho$ at the interface nodes is then obtained by adding the contributions from the level sets present at a certain node by the following steps:

1. At each interface node, find the level set with the highest stored energy: $\max\left(E_{\mathrm{s},k}\right) \Rightarrow \phi_i, \quad k \in \widetilde{N}_\phi$
2. Define $\boldsymbol{v}_\rho = \sum_j m[\![E_\mathrm{s}]\!]_{ij}\ \boldsymbol{n}_j\left(\boldsymbol{x},t\right), \quad j \neq i, \quad i,j \in \widetilde{N}_\phi$

where the summation is performed over all level sets contained in $\widetilde{N}_\phi$. This approach to evaluating $\boldsymbol{v}_\rho$ is similar to that proposed in [40] where, however, the contribution at all nodes from all level sets is used in the summation since interface nodes are not defined.

4.2 Modeling of grain nucleation

One of the appealing features of the level set method is its ability to directly handle topological changes such as the appearance and disappearance of individual level sets. In the present model, a grain represented by the level set ϕ_j is considered as disappeared once $\phi_j \leq 0$ everywhere. As this occurs, the disappeared level set is removed from subsequent time steps to promote computational efficiency.

Nucleation of recrystallized grains generally occur at sites of high stored energy in the microstructure. These sites are primarily found at grain boundary triple junctions, along grain boundaries, at particle inclusions and at slip bands in the grain interiors. In the present model, a nucleation criterion based on the local dislocation density is used. By this approach, nucleation is initiated once a critical dislocation density ρ_c is reached at some site in the microstructure.

Addition of level sets due to nucleation is performed by identifying locations where the nucleation criterion is met, i.e. the corresponding nodal points are located. A new signed

distance function is created as a concentric circular contour, with a set radius, around the nucleation center.

The nucleation event itself, in terms of nuclei present at a given microstructure state, is in the present model assumed to be governed by a rate of nucleation law on the form

$$\dot{n}\left(T, \dot{\varepsilon}_{\text{eff}}\right) = c_{\text{n}}\left(T\right) \dot{\varepsilon}_{\text{eff}}^{\text{p}} \left(\frac{-Q_{\text{n}}}{RT}\right) \tag{18}$$

where n is the number of nuclei per unit volume, $c_{\text{n}}\left(T\right)$ is temperature dependent parameter, controlling the extent of nucleation, and Q_{n} is the activation energy for nucleation. Driven by the rate of macroscopic plastic deformation, eq. (18) represents a constant rate of nucleation law, corresponding to the proportional nucleation model in [41, 42], also employed in [43, 44]. It should be noted, however, that the rate of nucleation in the present model is constant at a given temperature but will change with changing temperature. Alternative rate-of-nucleation laws could be employed directly within the present model framework by replacing eq. (18).

5 Interface reconstruction

The FE-based level set modeling of interfaces involves a diffuse representation of the boundaries in the sense that FE nodal points do not necessarily coincide with the interfaces. This leads to some issues, for example when boundary conditions need to be applied along the interfaces. In the present work, an interface reconstruction methodology is suggested and employed to allow additional flexibility in treating phenomena such as discontinuities of field variables across the boundaries.

As discussed in Section 2.2, standard level set implementations do not provide the exact localization of junction points between multiple level sets, typically found at grain boundary triple junctions. This is also addressed by the proposed interface reconstruction.

It can be noted that when representing for example displacement discontinuities at the interfaces in terms of level sets, extended finite element methods (XFEM) is sometimes employed [45]. However, also XFEM requires interpolation of the location of the interfaces during numerical integration of the field variable under consideration. XFEM also further adds to the computational effort by adding additional degrees of freedom to the model.

In the present work, displacement discontinuities at the grain boundaries are not required since no relative movement between adjacent grains – such as grain boundary sliding – is considered. In contrast, jumps in the scalar stored energy field are considered as well as the position and configuration of interface triple junctions. Hence, a methodology based on interface interpolation and remeshing is adopted here.

The interface reconstruction is performed through the following procedure: After updating the positions of the interfaces by solving eq. (17), the interfaces are located by

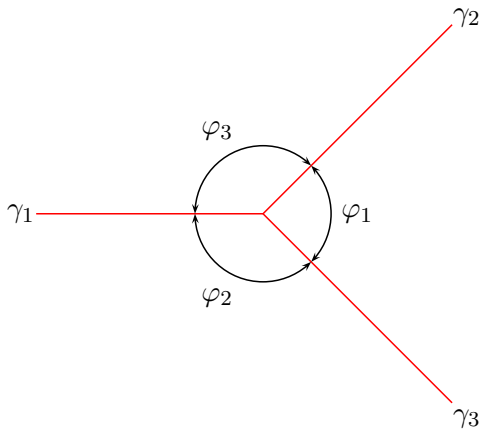

Figure 3: Schematic illustration of three grain boundaries, with different interface energies γ_1, γ_2 and γ_3, meeting at a triple junction.

interpolation in the FE mesh. Elements cut by one or more interfaces are conveniently identified by finding those elements where the nodal level set values fulfill the criterion

$$\min(\phi_j) \cdot \max(\phi_j) \leq 0 \quad \text{for any} \quad \phi_j, \quad j = 1...N_\phi \tag{19}$$

If more than two level sets fulfill this criterion in a single element, the element contains a junction.

Once the elements that contain interfaces are identified, the interface crossing points at the element edges are found by interpolation. This allows definition of interface line segments between the crossing points in each element. This is a direct geometric representation of the modeled grain boundary, also used in the level set reinitialization discussed in Section 2.2.

Elements that contain triple junctions require some special attention. The precision with which the junction is localized depends on the mesh or grid resolution in the region surrounding the junction point. But no matter how fine the resolution is, the junction point will end up somewhere in the interior of a single element, without being exactly positioned. The exception being the unlikely event that a junction by chance precisely coincides with a grid point.

Considering the triple junction illustrated in Fig. 3, the Herring equation [46] dictates the triple junction equilibrium configuration to fulfill

$$\frac{\gamma_1}{\sin(\varphi_1)} = \frac{\gamma_2}{\sin(\varphi_2)} = \frac{\gamma_3}{\sin(\varphi_3)} \tag{20}$$

If all involved interface energies are equal, the grain boundaries will meet at angles $\varphi_1 = \varphi_2 = \varphi_3 = 120°$.

In the present implementation, the triple junctions are reconstructed in the corresponding elements by identifying the junction as the isogonic point[1] in the triangle defined by the three interface crossing points along the element edges. The isogonic point is found as the point that minimizes the total distance from the three triangle vertices to the point. The present method for triple junction reconstruction is illustrated in Fig. 4 and involves the following steps:

1. Identify an element containing a triple junction, Fig. 4a.
2. Interpolate the three interface crossing points A, B and C along the element edges, Figs. 4a and 4b.
3. Calculate the isogonic point D, defined by the triangle ABC, Fig. 4b.
4. Define interface segments between the isogonic point D and each of the three crossing points A, B and C, Fig. 4c.

Reconstructing triple junctions by means of isogonic points ensures that the 120° equilibrium angles are present between the joining interfaces at the junction. It should also be noted that by using an appropriately refined mesh near triple junctions, the junction reconstruction is performed within a very small region of the microstructure. The end result is clearly defined junction points, in contrast to standard level set implementations where artificial voids surround the junctions [24, 31].

Having achieved a definition of the grain boundaries at the current microstructure state in terms of interface segments, the length of these segments can be used to control the mesh resolution during subsequent remeshing. In the present model implementation, a target segment length l_{seg} is defined. All segments longer than this value are divided and all segments shorter than the target value are merged. The vertices of the interface segments are used as prescribed nodal positions to control adaptive meshing through constrained Delaunay triangulation using the *Triangle* software [47]. This is further discussed in relation to the simulation examples in Section 7.

To summarize, the present level set implementation with interface reconstruction has advantages in terms of:

1. Allowing boundary conditions to be applied at interfaces. This is used in the consideration of dislocation density gradients in Section 6.
2. Distinct localization of triple junction points.
3. Ensuring that grain boundaries meet with 120° dividing angles at triple junctions, i.e. respecting the equilibrium configuration given by eq. (20).

[1]The isogonic point is also known as the Fermat point or the Torricelli point.

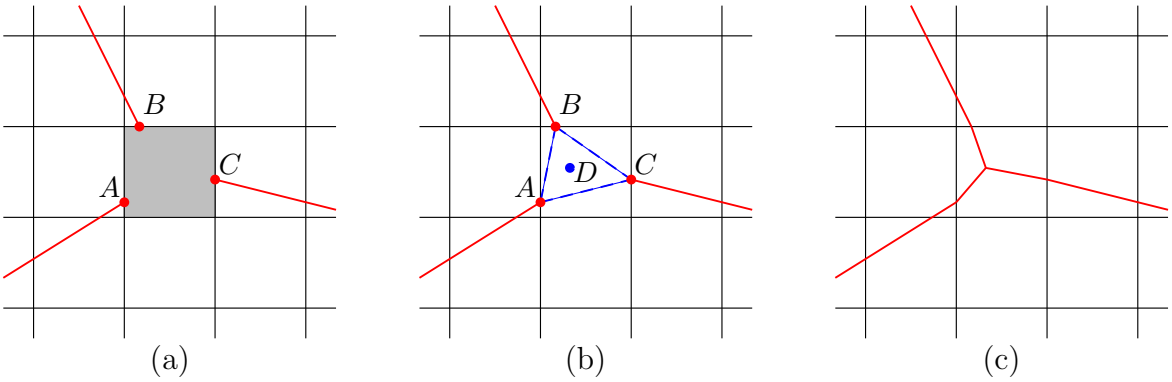

Figure 4: Schematic illustration of the steps whereby a triple junction is located using the isogonic point of a triangle ABC. a) Interpolation of the location of grain boundaries – indicated by red lines – and identification of the crossing points A, B and C. The shaded element is identified to contain a triple junction. b) Definition of a triangle ABC in the element that contains the triple junction and subsequent definition of the isogonic point D within the triangle ABC. c) Interface definition at the reconstructed triple junction by three new interface segments.

4. Allowing evaluation of the interface velocity due to bulk energy differences across the interface, Section 4.1.

5. The interface segments can be used for level set reinitialization, as discussed in Section 2.2.

6. Adaptive mesh control can be performed since the interface segmentation can be used to control the element size along the boundaries. This is done in the present work by setting the target segment length l_{seg}, further used in Sections 7 and 8.

7. Quantities pertaining to individual level sets/grains can be treated on a per-element basis since each element belong uniquely to a single level set.

8. Convenient calculation of domain areas, i.e. grain sizes in the present case, by summation of the element areas belonging to an individual level set.

9. Facilitated post-processing of calculation results. A direct graphical representation of the grain boundaries is available, using the interface segments.

6 Modeling of polycrystal plasticity and heterogeneous dislocation density distributions

In order to describe the evolution of plasticity in a polycrystalline material, the evolution of the dislocation density inside a single grain due to an applied macroscopic plastic strain

is herein assumed to follow the Kocks-Mecking relation

$$\frac{d\rho_j}{d\varepsilon^{\mathrm{p}}_{\mathrm{eff},j}} = k_1\sqrt{\rho_j} - k_2\rho_j, \quad j = 1...N_\phi \tag{21}$$

where ρ_j and $\varepsilon^{\mathrm{p}}_{\mathrm{eff},j}$ is the dislocation density and the effective plastic strain in grain j, respectively [48, 49, 50, 51, 52]. Following [50, 51], the parameter k_1 is related to the athermal accumulation of immobilized dislocations due interaction between dislocations, i.e., due to obstacles with a spacing proportional to the inter-dislocation spacing $(\rho_j)^{-1/2}$. The parameter k_2 is associated with recovery due to dislocation annihilation processes. Whereas the parameter k_1 is constant, the parameter k_2 is usually a function of temperature and strain rate [48, 49, 50, 52].

Athermal dislocation accumulation due to the presence of grain boundaries – which are obstacles with a spacing greater than the inter-dislocation spacing – can be considered by adding a third term, here denoted by k_j, to eq. (21) which then appears as

$$\frac{d\rho_j}{d\varepsilon^{\mathrm{p}}_{\mathrm{eff},j}} = k_1\sqrt{\rho_j} - k_2\rho_j + k_j, \quad j = 1...N_\phi \tag{22}$$

This parameter is usually taken as being proportional to $(bd)^{-1}$, where d is the grain size. In the present model, however, the distance information provided by the level sets – which by reinitialization maintain the property of a signed distance function – can be utilized to formulate

$$k_j(\phi_j) = \frac{1}{b\max(\phi_j)} f(\phi_j) \quad \text{for all} \quad j = 1...N_\phi \quad \text{where} \quad \phi_j > 0 \tag{23}$$

The presence of $\max(\phi_j)$ in the denominator of eq. (23) provides a measure of the grain size since the highest value of each level set function gives the maximum distance, within the grain, from the grain boundary. This maximum distance is an indication of the grain radius, with a precision partly depending on the mesh resolution.

Also introduced in eq. (24), the function $f(\phi_j)$ controls the increased impact of the k_j term on the dislocation density evolution in the vicinity of grain boundaries. This is achieved by formulating the function $f(\phi_j)$ as

$$f(\phi_j) = r_{\min} + (1 - r_{\min}) \exp\left(-w\frac{\phi_j}{\max(\phi_j)}\right), \quad \phi_j > 0 \tag{24}$$

The parameter $0 \leq r_{\min} \leq 1$ controls the influence of k_j in the grain interior, away from the boundary, and the parameter w controls how fast the influence of k_j decays when moving away from the grain boundary. The gradient in the dislocation density distribution due to dislocation pile-up at the grain boundaries is controlled by w. The influence of the parameters $r_{\min}$ and w is illustrated in Fig. 5.

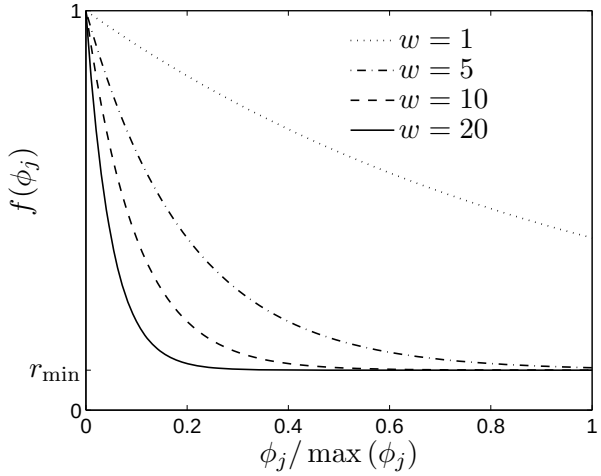

Figure 5: Illustration of the influence of the parameters $r_{\min}$ and w on the scaling function $f(\phi_j)$, $1 \leq j \leq N_\phi$, cf. eq. (24). Note that $f = 1$ at the grain boundary, where $\phi_j / \max(\phi_j) = 0$, and $f \to r_{\min}$ at the grain center where $\phi_j / \max(\phi_j) = 1$.

In the present work the dependence of dislocation accumulation on the distance to the grain boundary is for simplicity taken to follow the simple exponential format chosen in eq. (24). More elaborate formulations are conceivable, where k_j depends in other ways on ϕ_j. For such modeling, it is noted that the appearance of the dislocation density distribution in real microstructures can be determined experimentally from electron backscatter diffraction (EBSD) data, as reported in [53, 54, 55]. It can also be noted that the present modeling framework does not restrict alternative forms of eq. (24).

Considering dislocation density gradients by introducing k_j in eq. (22) will influence the microstructure evolution as well as the homogenized macroscopic material response to deformation. In [56], the present author identified another approach to modeling dislocation density gradients in relation to microstructure evolution. This is achieved by considering the dislocation density evolution as a reaction/diffusion system, separating between mobile and immobile dislocations. However, seeking to enhance computational efficiency and utilizing the distance information embedded into the level set framework, the approach related to eqs. (22)-(24) is adopted in the present work. In [56] it was also found that the introduction of dislocation density gradients in mesoscale polycrystal models – as is also the setting in the present case – will yield a Hall-Petch dependence of the macroscopic, homogenized, flow stress on the average grain size. This is maintained by the present approach to dislocation density gradient modeling.

The dislocation density gradients will also provide additions to the modeling of recrystallization on the scale of the grain microstructure. With a nucleation criterion based on a critical dislocation density threshold value, as discussed in Section 4.2, the presence of

dislocation density gradients will provide the appropriate nucleation sites. The modeled nucleation will naturally take place primarily along grain boundaries where the dislocation density is the highest, in accordance with experimental observations [2].

Fig. 6 illustrates how the evolving dislocation density distribution is influenced by eq. (24) when the dislocation density in each grain is initiated from a random normal distribution with mean 10^{11} m^{-2} and standard deviation of 10^{10} m^{-2}. Additional parameters are defined in Section 8 as Fig. 6 is shown here only for illustration purposes. The illustrations in Fig. 6 are obtained at a strain of 0.1.

The different distributions in Fig. 6 are obtained by setting $r_{\min} = 0.5$ and varying the parameter w. As shown in Fig. 6, the dislocation density distribution will be increasingly concentrated along the grain boundaries as the value of w is increased, consistent with the behavior shown in Fig. 5.

From Fig. 6 it can also be noted that a higher dislocation density is maintained throughout the interior of smaller grains. This is a replication of grain boundary influence becoming more dominant as smaller grains are considered. In contrast, as larger grains are considered, the difference in dislocation density becomes greater when comparing the grain centers and the grain boundary regions. These observations are related to the macroscopic flow stress exhibiting a Hall-Petch-type of dependence on the grain size [56].

The dislocation content, in terms of geometrically necessary dislocations, can be related to gradients in the lattice orientation within individual grains. Using EBSD techniques, such orientation distributions and related dislocation content have been quantified experimentally in, for example, [57, 58, 59, 60]. In [60] it is observed that there is a clear trend for higher dislocation density in smaller grains, as also indicated in Fig. 6. Regarding the the appearance of dislocation density gradients, it can be noted from the experimental observations in [57, 59] that an exponential function, such as the one proposed in eq. (24), captures the dislocation density variation near grain boundaries quite well. From the experimental studies in [58, 59] it appears that the high level of dislocation density near grain boundaries extend into the grains over roughly 10 % of the grain radius. This width can be represented by the parameter w in eq. (24).

Denoting the second-stage hardening rate and the saturation level of the flow stress at steady state by Θ_{II} and σ_{s}, respectively, the parameters k_1 and k_2 in eq. (22) can be evaluated from experimental data by considering the relations

$$\Theta_{\mathrm{II}} = \frac{1}{2}\alpha\mu b k_1 \quad \text{and} \quad \sigma_{\mathrm{s}} = \alpha\mu b\frac{k_1}{k_2} \tag{25}$$

where α is a parameter in the order of unity, related to the strength of dislocation interactions [50, 12]. The parameter k_1 will in such results contain the combined influence of k_1 and k_j in eq. (22). The separate influence of the k_j parameter is, due to lacking experimental data, heuristically added in the present model to reflect grain boundary influence. The

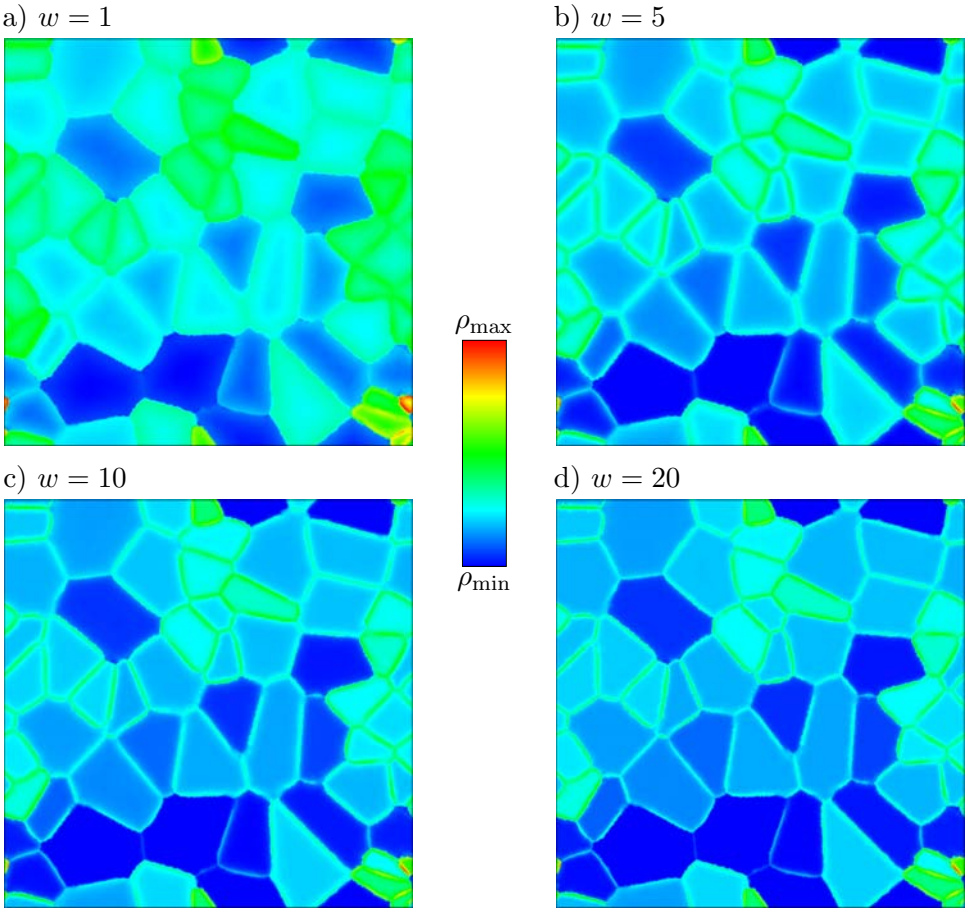

Figure 6: Illustration of the influence of eq. (24) on the distribution of dislocation density in a simulated polycrystal at a strain of 0.1. The parameter $r_{\min}$ is held constant at $r_{\min} = 0.5$ while the parameter w is varied. a) $w = 1$, b) $w = 5$, c) $w = 10$ and d) $w = 20$. Note the concentration of dislocation density along the grain boundaries.

distinction between dislocation accumulation due to obstacles of different sizes requires additional experimental input, for example from EBSD measurements, as mentioned earlier in this section. The function k_j and the related parameters $r_{\min}$ and w in eq. (24) are introduced in the present model to illustrate one convenient way of introducing dislocation density gradients, with advantage being taken of the information contained in the level set formulation. Another approach is the reaction-diffusion modeling of dislocation density evolution, proposed in [56].

The saturation level of the macroscopic flow stress at steady state is in [61, 52] observed to satisfy a proportionality according to

$$\log\left(\frac{\sigma_{\mathrm{s}}}{\mu}\right) \propto g\left(T, \dot{\varepsilon}^{\mathrm{p}}_{\mathrm{eff}}\right) \tag{26}$$

where g is a function, varying with temperature and the rate of macroscopic effective plastic strain, according to

$$g\left(T, \dot{\varepsilon}^{\mathrm{p}}_{\mathrm{eff}}\right) = \frac{k_{\mathrm{B}}T}{\mu b^3} \ln\left(\frac{10^7}{\dot{\varepsilon}^{\mathrm{p}}_{\mathrm{eff}}}\right) \tag{27}$$

where k_{B} is the Boltzmann constant. By fitting against experimental data, the steady-state saturation stress σ_{s} may now be determined by eq. (26).

In addition, following [50], the macroscopic flow stress, related to an average dislocation density $\bar{\rho}$ can be determined from

$$\hat{\sigma} = \frac{1}{2}\mu b\sqrt{\bar{\rho}} \tag{28}$$

To obtain the average dislocation density of a polycrystalline aggregate, a Taylor-type assumption is made whereby increments in effective plastic deformation is taken to be equally distributed among the grains. This allows a volume averaging of the dislocation density to be performed by homogenizing of the plastic power $\dot{w}^{\mathrm{p}}$ according to

$$\dot{w}^{\mathrm{p}} = \hat{\sigma}\dot{\varepsilon}^{\mathrm{p}}_{\mathrm{eff}} = \frac{1}{V}\sum_j \int_j \dot{w}^{\mathrm{p}}_j dV = \frac{1}{V}\sum_j \int_j \hat{\sigma}_j \dot{\varepsilon}^{\mathrm{p}}_{\mathrm{eff},j} dV \tag{29}$$

where V_j i the volume of grain j and V is the total volume of the domain under consideration. Using $\hat{\sigma}_j = 1/2\mu b\sqrt{\rho_j}$ and $\dot{\varepsilon}^{\mathrm{p}}_{\mathrm{eff}} = \dot{\varepsilon}^{\mathrm{p}}_{\mathrm{eff},j}$, the average dislocation density is obtained as

$$\sqrt{\bar{\rho}} = \frac{1}{V}\sum_j \int_j \sqrt{\rho_j} dV \tag{30}$$

A dependence of the macroscopic flow stress on the strain rate is introduced, following [48], by adding a strain rate sensitivity to eq. (28) according to

$$\sigma = \hat{\sigma}\left(\frac{\dot{\varepsilon}^{\mathrm{p}}_{\mathrm{eff}}}{\dot{\varepsilon}_{\mathrm{ref}}}\right)^{\eta} \equiv \frac{1}{2}\mu b\sqrt{\bar{\rho}}\left(\frac{\dot{\varepsilon}^{\mathrm{p}}_{\mathrm{eff}}}{\dot{\varepsilon}_{\mathrm{ref}}}\right)^{\eta} \tag{31}$$

The strain rate sensitivity of the plasticity model is now controlled by the reference strain rate $\dot{\varepsilon}_{\text{ref}}$ and the strain rate sensitivity parameter η, whereas the temperature dependency lies in the shear modulus μ and in the k_2 parameter, as determined from the saturation stress σ_{s} according to eqs. (25) and (26).

7 Grain growth kinetics resulting from the simulations

In order to illustrate how grain growth kinetics according to eqs. (9) and (10) is captured by the present model, a single spherical grain embedded into a matrix material is considered, cf. Fig. 7. Such a simplified model is useful to investigate the model representation of interface curvature.

Considering eqs. (9)-(10), the radial velocity of the single spherical grain of radius R can be written as

$$\dot{R} = \frac{dR}{dt} = m[\![E_{\text{s}}]\!] - m\frac{2\gamma}{R} \tag{32}$$

where, compared to eqs. (9)-(10), the vectorial notation is dropped for convenience since the velocity is confined to the radial direction of the sphere and the curvature is obtained from $\kappa = 2/R$. Under purely curvature-driven grain boundary migration the grain will shrink whereas the presence of a stored energy difference $[\![E_{\text{s}}]\!]$ across the grain boundary may contribute enough driving force to allow grain growth to take place.

Considering purely curvature-driven motion, the first term on the right-hand side of eq. (32) vanishes, and the remaining expression can be integrated to obtain

$$R\,(t) = \left(R_0^2 - 4m\gamma t\right)^{1/2} \tag{33}$$

where R and R_0 are the current and initial radii of the grain, respectively, also cf. [62]. To make a comparison between this analytical behavior and the model response, material parameter values are chosen as $m = 1.86 \times 10^{-11}$ m^3·N^{-1}·s^{-1} and $\gamma = 0.625$ J·m^{-2}, pertaining to pure copper at $T = 875$ K. These parameters are discussed further in Section 8.

The one-grain simulations are performed on a 500×500 μm 2D domain with periodic boundary conditions along the outer edges. Domain discretization is performed, using three-node elements with linear interpolation. Advantage is taken of the interface segment length l_{seg} – obtained from the interface reconstruction discussed previously in Section 5 – as a controlling parameter for adaptive mesh refinement, performed in each time step by constrained Delaunay triangulation.

With $R_0 = 100$ μm, the analytical result from eq. (33) is in Fig. 7 compared to simulation results, obtained using three different mesh resolutions. The different meshes are obtained by varying the value of l_{seg} with values stated in Fig. 7. The results indicate that the level of mesh refinement, required in order to properly capture curvature-driven interface motion, is obtained for $l_{\text{seg}} = 3.5$ μm.

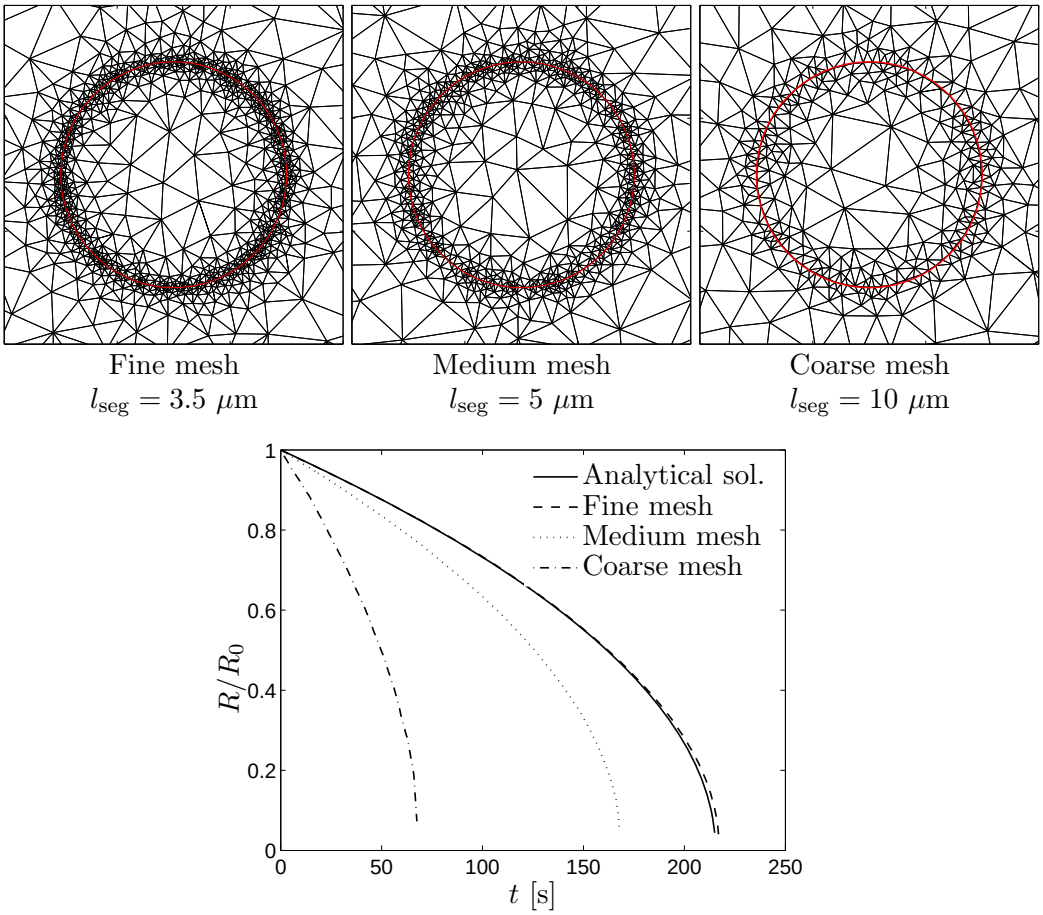

Figure 7: The three top figures show different mesh refinements in a 300×300 μm domain around a circular level set corresponding to a single grain, embedded in a matrix material. The graph below shows the normalized grain radius as the grains shrink due to purely curvature-driven motion. The solid line shows the analytical solution, as obtained from eq. (33), and the different dashed lines show the simulation result for the three different mesh resolutions. The graph shows the significance of proper mesh resolution to capture interface curvature.

Table 1: Material parameters pertaining to pure copper.

Parameter	Description	Value	Reference
T_m	Melting temperature	1356 K	[65]
α	Dislocation junction strength	0.35	[64]
Θ_II	Stage II strain hardening rate	1.1×10^9 Pa	[64]
η	Strain rate sensitivity parameter	0.0222	[64]
s_1, s_2	Saturation stress fitting parameters	-2.271, -1.654	[64]
b	Magnitude of the Burgers vector	0.256 nm	[66]
γ	Grain boundary energy	0.625 J·m^{-2}	[65]
$\dot{\varepsilon}_\mathrm{ref}$	Reference strain rate	4.5×10^{-7} s^{-1}	[64]
Q_m	Activation energy for grain boundary migration	104 kJ·mol^{-1}	[67]
Q_n	Activation energy for nucleation	261 kJ·mol^{-1}	[68]
δD_gb	Grain boundary width and diffusivity	5×10^{-5} m^3·s^{-1}	[67]
β	Scaling parameter in the grain boundary mobility	0.5	[64]
V_m	Molar volume	7.11×10^{-6} m^3	[69]

8 Application to dynamic discontinuous recrystallization in pure Cu

Taking pure copper as example material, parameter values have to be established accordingly. In [63], the shear modulus is given a temperature dependence on the form

$$\mu\left(T\right) = 35.4 \times 10^9 \left[1 - 0.5\left(\frac{T - 300}{T_\mathrm{m}}\right)\right] \quad \mathrm{MPa} \tag{34}$$

where T_m is the melting temperature.

In [64], the temperature and strain rate dependent saturation stress in eqs. (26)-(27) is fitted against experimental data, resulting in

$$\log\left(\frac{\sigma_\mathrm{s}}{\mu}\right) = s_1 g + s_2 \tag{35}$$

where values of the fitting parameters s_1 and s_2 are given in Table 1. Further considering the experimental data on hot compression of pure Cu provided in [68], an initial artificial microstructure RVE with 52 grains is generated through Voronoï tessellation to provide a simulation model with an average grain size of 78 μm, cf. Fig. 8. The initial Voronoï structure is run for a few time steps under purely curvature-driven grain boundary motion to equilibrate the triple junction angles and obtain a more realistic grain boundary configuration. The RVE has outer dimensions of 500×500 μm and periodic boundary conditions are applied along the outer edges.

The dislocation density distribution is initiated by randomly prescribing to each grain a dislocation density from a normal distribution with mean 10^{11} m^{-2} and standard deviation 10^{10} m^{-2}. The dislocation density is initially homogeneously distributed within each grain and gradients in the distribution will develop due to the formulation adopted in eqs. (22)-(23).

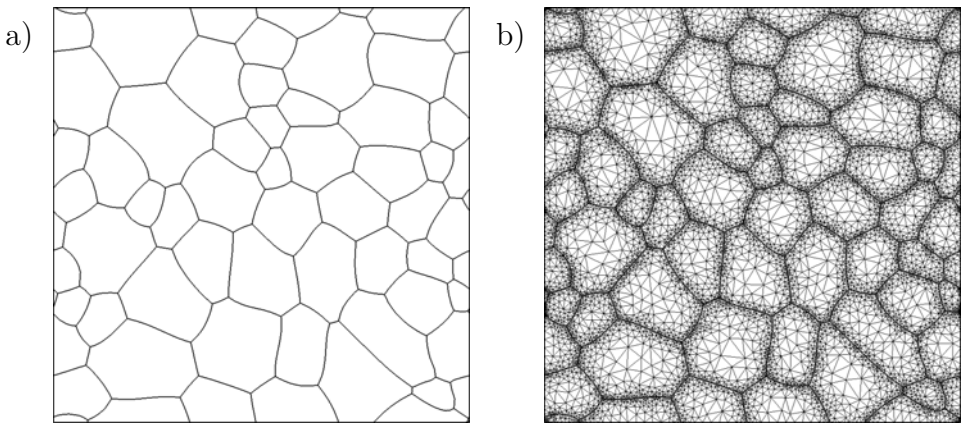

Figure 8: Artificial 2D microstructure used in the simulations. The RVE has outer dimension of 500×500 μm and periodic boundary conditions are applied on the outer boundary. The initial microstructure consists of 52 grains, with an average grain size of 78 μm. a) Grain boundaries, represented by interface segments. b) Mesh discretization from a Delaunay triangulation with approximately 20,000 elements.

Table 2: Values of the only two temperature dependent calibration parameters in the model. T is the absolute temperature and ρ_{c} and c_{n} is the critical dislocation density for nucleation and a parameter influencing the rate of nucleation, cf. eq. (18), respectively.

T [K]	ρ_{c} [m^{-3}]	c_{n}
775	3.8×10^{14}	20.5×10^{20}
875	1.5×10^{14}	11.4×10^{18}
975	5.8×10^{13}	38.4×10^{16}

As in the previous one-grain example simulations, Three-node elements with linear interpolation are used, cf. Fig. 8. Adaptive remeshing, using the interface segment length $l_{\mathrm{seg}} = 3.5$ μm for controlling the element size at the grain boundaries, is performed in each time step. This value of l_{seg} is chosen based on the results obtained in Section 7.

Considering the experimental data on hot compression of pure Cu presented in [68], the homogenized macroscopic response of the present model can be evaluated. To achieve this, the only two remaining parameters to be defined are the critical threshold value of dislocation density at the onset of recrystallization, ρ_{c}, and the coefficient c_{n} in the rate of nucleation law, cf. eq. (18). The parameter values used at the temperatures under consideration are given in Table 2. As stated in [68], a macroscopic strain rate of $\dot{\varepsilon}^{\mathrm{p}}_{\mathrm{eff}} = 2 \times 10^{-3}$ s^{-1} was used in the simulations to comply with the experimental data.

The results from the simulations are shown in Fig. 9 together with experimental from [68]. The macroscopic flow stress behavior that is obtained from the simulations, shown in Fig. 9, can be seen to capture the transition from single-peak flow at $T = 775$ K into

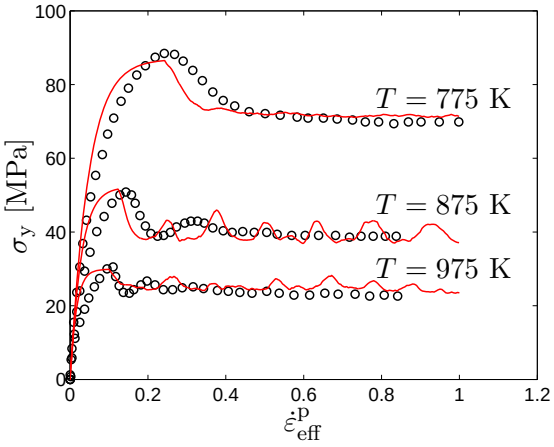

Figure 9: Macroscopic flow stress as a function of macroscopic effective plastic strain at different temperatures. The solid lines show simulation results, obtained in the present work, and the circles show experimental data on hot compression of pure Cu, from [68].

Table 3: Steady-state grain sizes obtained in the simulations at three different temperatures, cf. Fig. 9a, compared to those obtained experimentally in [68], cf. Fig. 9b. Grain size values are given in microns.

T [K]	Simulation, present work	Experiment, from [68]
775	19	14
875	39	34
975	56	57

multiple-peak flow as the temperature is increased. This transition is in agreement with the trends shown in the experimental results, indicated by the small circles in Fig. 9. The increasing oscillations found as the temperature is increased are characteristic for materials undergoing dynamic discontinuous recrystallization. At lower temperatures, or higher strain rates, a single cycle of recrystallization does not have time to finish before the next cycle sets in. These parallel waves of recrystallization damp out the flow stress oscillations. In contrast, at higher temperatures or at lower strain rates, each cycle of recrystallization is more or less allowed to finish prior to the next. This results in the serrations of the macroscopic flow stress curve.

Following the experimental conditions in [68], an initial average grain size of 78 μm was used in the simulations. The steady-state grain sizes, obtained at the end of the deformation process at each temperature, are given in Table 3 together with the experimental values. A reasonable agreement is found between the simulated steady-state grain sizes obtained from the simulations in the present work and the experimental values from [68].

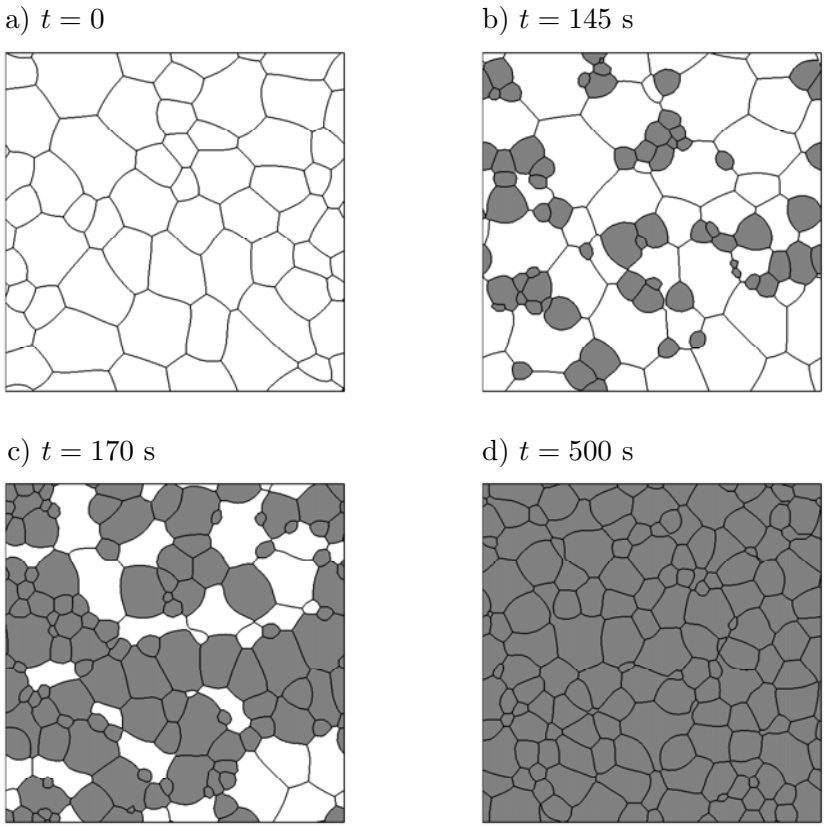

Figure 10: Appearance of the microstructure at different stages during dynamic recrystallization at $T = 875$ K, cf. Fig. 9a.

DOI: 10.1088/0965-0393/21/8/085012

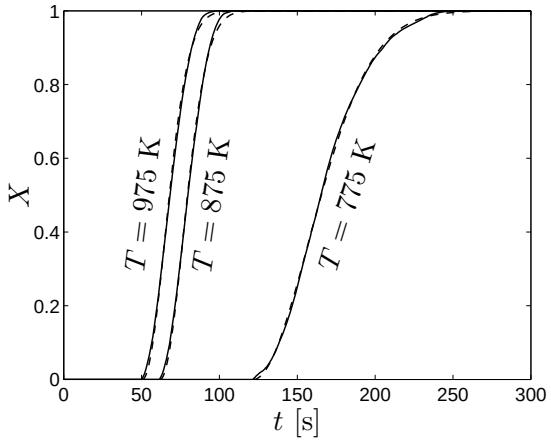

Figure 11: Recrystallization kinetics represented by the recrystallized fraction as a function of time at three different temperatures. Solid lines show simulation results and dashed lines show fits of the Avrami relation in eq. (36).

8.1 Correspondence with JMAK theory

The progress of recrystallization is classically described by the Kolmogorov-Mehl-Avrami-Johnson KJMA relation through the Avrami equation

$$X = 1 - \exp\left(-Bt^n\right) \tag{36}$$

where X is the recrystallized fraction and where the two parameters B and n describe the recrystallization kinetics [70, 71, 72]. Although established under several simplifying assumptions, eq. (36) is widely used to quantify recrystallization kinetics.

Fig. 11 shows the recrystallized fraction as a function of time for the three different processing temperature presently under consideration, cf. Fig. 9. The solid lines show simulation results and the dashed lines show fits of the Avrami relation in eq. (36), obtained by least-squares fitting. The values of the Avrami exponent n, resulting from the fitting procedure, lie in the range between 1.9 at $T = 775$ K and 2 at $T = 975$ K. The first cycle of recrystallization, as shown in Fig. 11, thus appear with an Avrami exponent close to the value expected for 2D site saturated nucleation [2]. In the present simulations, nucleation occurs continuously at grain boundary sites whereas the KJMA relation is formulated under the simplifying assumption of randomly distributed nucleation sites.

9 Concluding remarks

In the present work, microstructure evolution in the presence of dynamic recrystallization is simulated on the mesoscale using a finite element-based level set formulation. Recognizing the level set approach to be a promising and relatively recent tool in mesoscale modeling

of polycrystals, new additions to standard level set formulations are proposed. These modifications include a interface reconstruction methodology, allowing boundary conditions to be prescribed along grain boundaries as well as distinct localization of triple junctions. The proposed interface reconstruction also provides the geometric configuration of the boundaries, meeting at the junctions. These features are absent in standard level set formulations where, for example, triple junctions are not distinctly localized.

Another addition to the level set modeling of polycrystal plasticity, proposed in the present work, is the treatment of gradients within the grains. Polycrystal plasticity is herein considered through the evolution of the dislocation density in the individual grains and the distance information contained in the level set formulation is used to capture the influence of grain boundaries on the distribution of the dislocation density. By this approach, dislocation pile-ups along grain boundaries are captured. With the dislocation density being concentrated along grain boundaries, the expected sites for nucleation of recrystallized grains emerge directly from the model, without having to be prescribed by additional model conditions.

The level set formulation is further equipped with a physically detailed model of dynamic recrystallization. The model is employed in simulations of thermomechanical processing of pure copper and the results are compared to experimental data, taken from the literature, with good agreement. It is shown that the proposed model captures all the salient features of dynamic recrystallization, including prediction of the recrystallized grain size and the transition from single-peak macroscopic flow to oscillatory flow stress behavior as the processing temperature is increased.

Some parameters are defined in the establishment of the present numerical model. There are basically two sets of parameters that come into play. These are those parameters related to the description of polycrystal plasticity and recrystallization kinetics (material parameters) and those related to the implementation of the level set formulation (algorithm parameters). The material parameters for pure copper are taken from the literature and stem from experiments. A such they are not free parameters but are defined by the material of choice. However, there is nothing in the model that restricts the type of metallic material that can be considered. The only material parameters available for fitting of the model is the critical dislocation density ρ_{c} and the nucleation parameter c_{n}, specified in Table 2. Both can be determined from experimental data on macroscopic flow stress behavior, possibly at different temperatures. The parameters $r_{\min}$ and w in eq. (24) can be included if dislocation density gradients are to be considered. These latter parameters can be adjusted to comply with experimental observations of, for example, misorientation gradients inside grains.

Regarding algorithm parameters, the significant parameter is the interface segment length l_{seg} which influences the mesh refinement at grain boundaries and thereby also the grain boundary kinetics. This parameter is calibrated by the procedure discussed in

Section 7, and illustrated in Fig. 7.

The present simulation model is initiated as a polycrystal RVE containing 52 grains. This may be considered as a relatively low number of grains and to ensure a statistically representative model, higher numbers could possibly be preferable. However, due to nucleation, the number of grains increases to a couple of hundred at the end of the deformation processes. As the primary objective of the present paper is to illustrate a modeling methodology, the chosen RVE size is considered sufficient for this purpose.

The proposed level set model, with interface reconstruction, naturally involves some computational effort. However, the present simulations run conveniently on a single CPU, using a standard desktop computer. Extending the model to 3D is certainly feasible, but will benefit from parallelization.

The characteristic features of DDRX, for example the serrated flow stress behavior shown in Fig. 9, have been achieved also in other mesoscale models of DDRX. For example by the present author in [12], using a 2D cellular automaton, by use of a 2D Monte Carlo Potts approach in [73] and by a mean field model in [74]. As mentioned in the introductory section of the paper, the finite element-based level set methodology has advantages, for example, in terms of properly capturing interface curvature and in the possibility to trace arbitrary geometries. In addition, finite deformations of the computational domain can be addressed. This is advantageous when using the mesoscale model in a multilevel setting, where deformation boundary conditions need to be communicated between modeling levels.

Previous work on level set modeling of recrystallization, such as in [27], has brought attention to some of the possibilities provided by this modeling approach. The present level set model of dynamic recrystallization adds further to the methodology by adding a more detailed description of polycrystal plasticity and recrystallization kinetics together with a study of the macroscopic, homogenized, material response. Further, novelties in the level set formulation itself are added. As examples: by the present approach, including interface reconstruction, intragrain gradients of field variables can be handled and grain boundary velocities can be evaluated directly at the interface nodes instead of in a diffuse region surrounding the grain boundaries. Boundary conditions can be prescribed at the grain boundaries and nucleation sites for DDRX emerge naturally from the model.

Acknowledgment

The author gratefully acknowledges funding from the Swedish Research Council under grant C0423101.

References

[1] R.D. Doherty, D.A. Hughes, F.J. Huphreys, J.J. Jonas, D. Juul Jensen, M.E. Kassner, W.E. King, T.R. McNelley, H.J. McQueen, and A.D. Rollett. Current issues in recrystallization: a review. *Mater. Sci. Eng.*, A238:219–274, 1997.

[2] F.J. Humphreys and M. Hatherly. *Recrystallization and related annealing phenomena*. Pergamon, New York, second edition, 2004.

[3] S. Gourdet and F. Montheillet. An experimental study of the recrystallization mechanism during hot deformation of aluminium. *Mater. Sci. Eng.*, A283:274–288, 2000.

[4] I. Mazurina, T. Sakai, H. Miura, O. Sitdikov, and R. Kaibyshev. Effect of deformation temperature on microstructure evolution in aluminum alloy 2219 during hot ECAP. *Mater. Sci. Eng.*, A486:662–671, 2008.

[5] T. Sakai, H. Miura, and X. Yang. Ultrafine grain formation in face centered cubic metals during severe plastic deformation. *Mater. Sci. Eng.*, A499:2–6, 2009.

[6] H. Hallberg. Approaches to modeling of recrystallization. *Metals*, 1:16–48, 2011.

[7] A.D. Rollett. Overview of modeling and simulation of recrystallization. *Prog. Mater. Sci.*, 42:79–99, 1997.

[8] M.A. Miodownik. A review of microstructural computer models used to simulate grain growth and recrystallisation in aluminium alloys. *J. Light Met.*, 2:125–135, 2002.

[9] D. Raabe. Discrete mesoscale simulation of recrystallization microstructure and texture using a stochastic cellular automation approach. *Mater. Sci. Forum*, 273-275:169–174, 1998.

[10] D. Raabe, P. Klose, B. Engl, K.-P. Imlau, F. Friedel, and F. Roters. Concepts for integrating plastic anisotropy into metal forming simulations. *Adv. Eng. Mat.*, 4(4):169–180, 2002.

[11] K.G.F. Janssens, D. Raabe, E. Kozeschnik, M.A. Miodownik, and B. Nestler. *Computational Materials Engineering*. Elsevier Academic Press, London, UK, 2007.

[12] H. Hallberg, M. Wallin, and M. Ristinmaa. Modeling of discontinuous dynamic recrystallization in pure Cu using a probabilistic cellular automaton. *Comp. Mater. Sci.*, 49(1):25–34, 2010.

[13] A. Soares, A.C. Ferro, and M.A. Fortes. Computer simulation of grain growth in a bidimensional polycrystal. *Scripta Metall. Mater.*, 19:1491–1496, 1985.

[14] H.J. Frost, C.V. Thompson, C.L. Howe, and J. Whang. A two-dimensional computer simulation of capillarity-driven grain growth: Preliminary results. *Scripta Metall. Mater.*, 22:65–70, 1988.

[15] K. Nakashima, T. Nagai, and K. Kawasaki. Scaling behavior of two-dimensional domain growth: Computer simulation of vertex models. *J. Stat. Phys.*, 57:759–787, 1989.

[16] A.C.F. Cocks and S.P.A. Gill. A variational approach to two dimensional grain growth

– I. Theory. *Acta Mater.*, 44:4765–4775, 1996.

[17] D. Weygand, Y. Bréchet, and J. Lépinoux. A vertex simulation of grain growth in 2D and 3D. *Adv. Eng. Mat.*, 3:67–71, 2001.

[18] D. Fan and L.-Q. Chen. Computer simulation of grain growth using a continuum field model. *Acta Mater.*, 45:611–622, 1997.

[19] D. Fan, S.P. Chen, and L.-Q. Chen. Computer simulation of grain growth kinetics with solute drag. *J. Mater. Res.*, 14:1113–1123, 1999.

[20] N. Moelans, B. Blanpain, and P. Wollants. An introduction to phase-field modeling of microstructure evolution. *Comp. Coupl. Phase Diagr. Thermochem.*, 32:268–294, 2008.

[21] I. Steinbach. Phase-field models in materials science. *Modelling Simul. Mater. Sci. Eng.*, 17:1–31, 2009.

[22] S. Osher and J.A. Sethian. Fronts propagating with curvature dependent speed: Algorithms based on Hamilton-Jacobi formulations. *J. Comput. Phys.*, 79:12–49, 1988.

[23] B. Merriman, J.K. Bence, and S.J. Osher. Motion of multiple junctions: A level set approach. *J. Comput. Phys.*, 112:334–363, 1994.

[24] H.-K. Zhao, B. Merriman, and S. Osher. A variational level set approach to multiphase motion. *J. Comput. Phys.*, 127:179–195, 1996.

[25] M. Bernacki, Y. Chastel, H. Digonnet, H. Resk, T. Coupez, and R.E. Logé. Development of numerical tools for the multiscale modelling of the recrystallization in metals, based on a digital material framework. In *AIP Conference Proceeding*, volume 908, pages 375–380, 2007.

[26] M. Bernacki, H. Resk, T. Coupez, and R.E. Logé. Finite element model of primary recrystallization in polycrystalline aggregates using a level set framework. *Modelling Simul. Mater. Sci. Eng.*, 17:1–22, 2009.

[27] M. Bernacki, R.E. Logé, and T. Coupez. Level set framework for the finite-element modelling of recrystallization and grain growth in polycrystalline materials. *Scripta. Mater.*, 64:525–528, 2011.

[28] R. Logé, M. Bernacki, H. Resk, L. Delannay, H. Digonnet, Y. Chastel, and T. Coupez. Linking plastic deformation to recrystallization in metals using digital microstructures. *Phil. Mag.*, 88:3691–3712, 2008.

[29] M. Elsey, S. Esedoḡlu, and P. Smereka. Diffusion generated motion for grain growth in two and three dimensions. *J. Comput. Phys.*, 228:8015–8033, 2009.

[30] M. Elsey, S. Esdoğlu, and P. Smereka. Large-scale simulations and parameter study for a simple recrystallization model. *Phil. Mag.*, 91(11):1607–1642, 2011.

[31] S.J. Ruuth. A diffusion-generated approach to multiphase motion. *J. Comput. Phys.*, 145:166–192, 1998.

[32] M. Sussman, P. Smereka, and S. Osher. A level set approach for computing solutions to incompressible two-phase flows. *J. Comput. Phys.*, 114:146–159, 1994.

[33] M. Sussman, E. Fatemi, P. Smereka, and S. Osher. An improved level set method for incompressible two-phase flows. *Comput. Fluids*, 27(5-6):663–680, 1998.

[34] R. Kimmel and J.A. Sethian. Computing geodesic paths on manifolds. *Proc. Natl. Acad. Sci. USA*, 95:8431–8435, 1998.

[35] J.A. Sethian and A. Vladimirsky. Fast methods for the Eikonal and related Hamilton-Jacobi equations on unstructured meshes. *Proc. Natl. Acad. Sci. USA*, 97(11):5699–5703, 2000.

[36] D. Turnbull. Theory of grain boundary migration rates. *J. Metals (N.Y.)*, 191(8):661–655, 1951.

[37] J. E. Burke and D. Turnbull. Recrystallization and grain growth. *Prog. Met. Phys.*, 3:220–292, 1952.

[38] C.W. Sinclair, C.R. Hutchinson, and Y. Bréchet. The effect of Nb on the recrystallization and grain growth of ultra-high-purity α-Fe: A combinatorial approach. *Metall. Mater. Trans.*, 38A:821–830, 2007.

[39] W.T. Read and W. Shockley. Dislocation models of crystal grain boundaries. *Phys. Rev.*, 78:275–289, 1950.

[40] M. Bernacki, Y. Chastel, T. Coupez, and R.E. Logé. Level set framework for the numerical modelling of primary recrystallization in polycrystalline materials. *Scripta. Mater.*, 58:1129–1132, 2008.

[41] P. Peczak and M.J. Luton. A Monte Carlo study of influence of dynamic recovery on dynamic recrystallization. *Acta Metall. Mater.*, 41(1):59–71, 1993.

[42] P. Peczak and M. J. Luton. The effect of nucleation models on dynamic recrystallization. II. Heterogeneous stored-energy distribution. *Phil. Mag. B*, 70(4):817–849, 1993.

[43] P. Ding, T. Inoue, S. Imatani, D.Y. Ju, and E. de Vries. Forging process simulation incorporating strain-induced phase transformation by the finite volume method. *Mater. Sci. Res. Int.*, 7(1):19–26, 2001.

[44] C. Zheng, N. Xiao, D. Li, and Y. Li. Mesoscopic modeling of austenite static recrystallization in a low carbon steel using a coupled simulation method. *Comp. Mater. Sci.*, 45:568–575, 2009.

[45] A. Simone, C.A. Duarte, and E. Van der Giessen. A generalized finite element method for polycrystals with discontinuous grain boundaries. *Int. J. Numer. Meth. Eng.*, 67:1122–1145, 2006.

[46] C. Herring. *The physics of powder metallurgy*, chapter 8, pages 143–179. McGraw-Hill, 1951.

[47] J.R.S. Shewchuk. Delaunay refinement algorithms for triangular mesh generation. *Comp. Geom.-Theor. Appl.*, 22(1-3):21–74, 2002.

[48] U. F. Kocks. Laws for Work-Hardening and Low-Temperature Creep. *J. Eng. Mater.-T. ASME*, 98(1):76–85, January 1976.

[49] H. Mecking and U.F. Kocks. Kinetics of flow and strain-hardening. *Acta Metall. Mater.*, 29:1865–1875, 1981.

[50] Y. Estrin and H. Mecking. A unified phenomenological description of work hardening and creep based on one-parameter models. *Acta Metall. Mater.*, 32(1):57–70, 1984.

[51] A.S. Krausz and K. Krausz, editors. *Unified Constitutive Laws of Plastic Deformation*, chapter 2, pages 69–106. Academic Press, 1996.

[52] U.F. Kocks and H. Mecking. Physics and phenomenology of strain hardening: the FCC case. *Prog. Mater. Sci.*, 48:171–273, 2003.

[53] F.J. Humphreys. Grain and subgrain characterisation by electron backscatter diffraction. *J. Mater. Sci.*, 36:3833–3854, 2001.

[54] S.-H. Choi and Y.-S. Jin. Evaluation of stored energy in cold-rolled steels from EBSD data. *Mater. Sci. Eng. A*, 371:149–159, 2004.

[55] S.S. Hazra, A.A. Gazder, and E.V. Pereloma. Stored energy of a severely deformed interstitial free steel. *Mater. Sci. Eng. A*, 524:158–167, 2009.

[56] H. Hallberg and M. Ristinmaa. Microstructure evolution influenced by dislocation density gradients modeled in a reaction-diffusion system. *Comp. Mater. Sci.*, 67:373–383, 2013.

[57] S. Sun, B.L. Adams, and W.E. King. Observation of lattice curvature near the interface of a deformed aluminum bicrystal. *Phil. Mag. A*, 80(1):9–25, 2000.

[58] M. Kamaya, A.J. Wilkinson, and J.M. Titchmarsh. Measurement of plastic strain of polycrystalline material by electron backscatter diffraction. *Nucl. Eng. Des.*, 235:713–725, 2005.

[59] M. Calcagnotto, D. Ponge, E. Demir, and D. Raabe. Orientation gradients and geometrically necessary dislocations in ultrafine grained dual-phase steels studied by 2D and 3D EBSD. *Mater. Sci. Eng.*, A527:2738–2746, 2010.

[60] P.D. Littlewood, T.B. Britton, and A.J. Wilkinson. Geometrically necessary dislocation density distributions in Ti-6Al-4V deformed in tension. *Acta Mater.*, 59:6489–6500, 2011.

[61] H. Mecking, B. Nicklas, N. Zarubova, and U.F. Kocks. A "universal" temperature scale for plastic flow. *Acta Metall. Mater.*, 34(3):527–535, 1986.

[62] M. Hillert. On the theory of normal and abnormal grain growth. *Acta Metall. Mater.*, 13:227–238, 1965.

[63] H.J. Frost and M.F. Ashby. *Deformation-Mechanism Maps*. Pergamon Press, 1982.

[64] D.G. Cram, X.Y. Fang, H.S. Zurob, Y.J.M. Bréchet, and C.R. Hutchinson. The effect of solute on discontinuous dynamic recrystallization. *Acta Mater.*, 60:6390–6404, 2012.

[65] H.S. Zurob, Y. Brechet, and J. Dunlop. Quantitative crietrion for recrystallization nucleation in single-phase alloys: Prediction of critical strains and incubation times. *Acta Mater.*, 54:3983–3990, 2006.

[66] H.S. Kim, Y. Estrin, E.Y. Gutmanas, and C.K. Rhee. A constitutive model for den-

sification of metal compacts: the case of copper. *Mater. Sci. Eng.*, 307:67–73, 2001.

[67] B. Derby. The dependence of grain size on stress during dynamic recrystallization. *Acta Metall. Mater.*, 39(5):955–962, 1991.

[68] L. Blaz, T. Sakai, and J.J. Jonas. Effect of initial grain-size on dynamic recrystallization of copper. *Met. Sci.*, 17(12):609–616, 1983.

[69] Y. Funamizu and K. Watanabe. Interdiffusion in the Al-Cu system. *Trans. Japan. Inst. Metals*, 12:147–152, 1971.

[70] M. Avrami. Kinetics of phase change, I. general theory. *J. Chem. Phys.*, 7:1103–1112, 1939.

[71] M. Avrami. Kinetics of phase change, II. Transformation-time relations for random distribution of nuclei. *J. Chem. Phys.*, 8:212–224, 1940.

[72] M. Avrami. Kinetics of phase change, III. Granulation, phase change and microstructure. *J. Chem. Phys.*, 9:177–184, 1941.

[73] P. Peczak. A Monte Carlo study of influence of deformation temperature on dynamic recrystallization. *Acta Metall. Mater.*, 43(3):1279–1291, 1995.

[74] F. Montheillet, O. Lurdos, and G. Damamme. A grain scale approach for modeling steady-state discontinuous dynamic recrystallization. *Acta Mater.*, 57:1602–1612, 2009.